energy&fuels

Article

pubs.acs.org/EF

Comparison of the Burning Characteristics of Indolene and Commercial Grade Gasoline Droplets without Convection

Yu Cheng Liu,* Anthony J. Savas, and C. Thomas Avedisian

Sibley School of Mechanical and Aerospace Engineering, Cornell University, Ithaca, New York 14853, United States

ABSTRACT: This study reports on the droplet combustion characteristics of indolene and a commercial 87 octane-rated (no ethanol) unleaded gasoline. The experiments are performed in an environment that simplifies the gas transport to one created entirely by the evaporation process (i.e., purely radial), thereby promoting spherical symmetry of the droplet burning process under normal atmospheric pressure air. In this way, the data characterize the base case of liquid fuel combustion, whereby the flame and droplet are concentric and spherical, and the soot aggregates that form collect in a shell-like structure between the droplet and flame. The tractable flame and sooting dynamics facilitate comparisons of the burning process, while at the same time they provide benchmark data that can be useful for model development. In the experiments reported here, the initial droplet diameters ranged from 0.47 mm to 0.59 mm, with an average of 0.53 ± 0.05 mm. Indolene and gasoline were found to display remarkably similar droplet evaporation rates. However, the sooting dynamics were substantially different. Indolene droplets produced soot shells that were somewhat thicker and resided farther from the droplet surface than the soot shells surrounding gasoline droplets. Furthermore, indolene flames were comparatively larger than gasoline flames. The highly multicomponent nature of both fuels did not result in noticeable preferential vaporization effects in the evolution of droplet diameter. These results show that indolene replicates some, though not all, of the droplet combustion properties of commercial gasoline.

1. INTRODUCTION

Indolene is a federal certification fuel that was developed to reproduce gasoline's emission qualities in practical engine tests. The importance of using indolene for engine tests is due to the fact that the composition of gasoline varies with regions and seasons. Indolene was formulated to mitigate this effect, thereby providing a more uniform bases of comparison. The word "indolene" originated from the trade name for a test fuel manufactured by Standard Oil Company,[1] and it was later adopted by Amoco/BP.[2]

In the U.S., indolene is more commonly referred to as a certification fuel that has passed the U.S. Federal Test Procedure (FTP) and can be used as a standard reference gasoline for engine emission testing. Similar to commercial gasoline, indolene is also produced from a petroleum refinery stream and thus consists of various hydrocarbons. To be certified as "indolene", the fuel has to pass a series of specification tests for physical and combustion properties,[3] such as distillation temperatures, density, Reid vapor pressure, sulfur content, aromatic and olefins contents, octane number, and net heating value. According to these specification regulations, manufacturers such as Amoco, Haltermann Solutions, or Chevron Phillips Chemical Company make certification fuels (Amoco/BP Indolene, TIER II EEE (HF-0437; EEE stands for Exhaust, Evaporative, and Emissions),[3] and Unleaded Gasoline (UTG-96),[4] respectively) that all meet the regulated properties. Cromas[5] compared the properties and particulate matter emissions of Amoco Indolene and Haltermann EEE fuel using a two-stroke direct-injection single cylinder research engine, and the results show that these two fuels are identical. Recognizing that many synonyms for indolene do exist, we hereafter use the term "indolene" to refer to this federal certification fuel. In the present study, "gasoline" refers to 87 octane rated fuel, as studied previously.[6]

Figure 1 shows a representative GC/MS trace for gasoline (a)[6] and indolene (b). Prominent constituents in indolene include C3 to C14 hydrocarbons, mostly normal-, iso-, and cyclo-alkanes and aromatics. These peaks are qualitatively consistent with a specification sheet[3] that indicates 70 vol % saturates, 2 vol % olefins, and 28 vol % aromatics in indolene. The gasoline GC/MS trace shows very similar behavior.

Although the GC/MS traces for gasoline and indolene are similar, they are not identical in all respects: the relative peak intensities for iso-octane and toluene in Figure 1 are considerably different for gasoline and indolene, and at a retention time of around 6 min, there is only one relatively weak peak for indolene, whereas for gasoline the prominent peak is due to ethylbenzene. Additional differences not visible in the GC/MS traces include indolene's comparatively low sulfur content.[7] These comparisons suggest differences in combustion performance (to be discussed later), especially for a conversion process that would involve preferential evaporation, species diffusion, and chemical reactions.

A number of studies have been reported on combustion of indolene in both spark ignition (SI) and compression ignition (CI) engines. For SI studies, the effect of additives (e.g., tert-butyl alcohol (TBA),[8] methyl-tert-butyl ether (MTBE),[8,9] methanol,[1] and ethanol[10−12]) on emissions has been examined. For CI engines, performance of indolene in a homogeneous charge compression ignition (HCCI) engine has also been studied.[13−15] Andersen et al.[16,17] used indolene (referred to as "EEE" gasoline) to investigate the effect of ethanol addition in gasoline on the distillation curve and vapor pressure. Meteghalchi and Keck[18] studied the flame velocity of indolene (research fuel RMFD-303); Abu-Isa[19] used indolene (HO-III) to evaluate the effect of adding ethanol and MTBE to gasoline on elastomer swelling; and Ganley and Springer[20] used leaded (HO 30) and unleaded (HO 0, clear) indolene to examine the effect of various

Received: May 7, 2012
Revised: July 22, 2012
Published: August 16, 2012

   dx.doi.org/10.1021/ef3007849 | *Energy Fuels* 2012, 26, 5740−5749

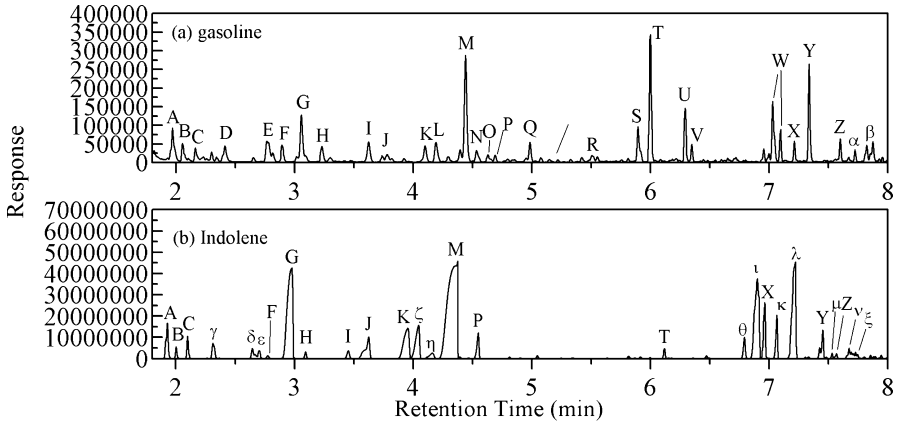

Figure 1. GC/MS traces and analysis for (a) gasoline (octane 87) and (b) indolene: A, 2-methylpentane; B, 3-methylpentane; C, hexane; D, methylcyclopentane, E, benzene; F, 3-methylhexane; G, iso-octane; H, *n*-heptane; I, methylcyclohexane; J, 2,4-dimethylhexane; K, 2,3,4-trimethylpentane; L, 3,3-dimethylhexane; M, toluene; N, 3-methylheptane; O, 1,3-dimethyl-cis-cyclohexane; P, 2,2,5-trimethylhexane; Q, *n*-octane; R, ethylcyclohexane; S, ethylbenzene; T, 1,3-dimethylbenzene; U, *p*-xylene; V, nonane; W, 1-ethyl-2-methyl-benzene; X, 1,2,3-trimethylbenzene; Y, 1,3,5-trimethylbenzene; Z, Indane; α, 1-ethyl-3,5-dimethybenzene; β, 1-methyl-2-(1-methylethyl)benzene; γ, 2,4-dimethylpentane; δ, cyclohexane; ε, 2,3-dimethylpentane; ζ, 2,3,3-trimethylpentane; η, 4-methylheptane; θ, propylbenzene; ι, 1-ethyl-3-methylbenzene; κ, 1-ethyl-4-methylbenzene; λ, 1,2,4-trimethylbenzene; μ, 3,7-dimethylnonane; ν, 1,3-diethylbenzene; ξ, 2-ethyl-1,3-dimethylbenzene.

engine parameters (e.g., spark timing, engine speed, air-fuel ratio) on particulate emission. While engine testing can provide useful information under realistic conditions specific to the engine design, the in-cylinder combustion dynamics, characterized by highly turbulent and swirling transport around the droplets, create significant challenges for modeling.

The characterization of real transportation fuels in a well controlled and modelable environment is important for validating some of the ingredients to predicting performance under more realistic conditions. For example, the combustion chemistry itself is independent of the transport dynamics and may be determined in a much simplified environment. Prevaporized (gaseous) fuels have particularly benefited from being developed in a combustion configuration for which the gas transport dynamics were well characterized. For example, shock tubes[21,22] give quantitative measurements of ignition delay, counter flow flames[23,24] characterize extinction strain rates, and jet-stirred[25] and premixed flow reactors[26] have provided species concentration data from the combustion process of prevaporized surrogate fuels in configurations that may be considered as "canonical" in the sense of the flow field being greatly simplified compared to the engine environment. The results still have much wider applicability.

For liquid fuels, the situation is different. We know of no study that has used a combustion configuration that captures the coupled phase equilibrium and evaporation behavior of indolene to develop a database that would be amenable to detailed numerical modeling for developing and testing the indolene combustion chemistry, or to develop a surrogate for this complex fuel. The present study reports on such an effort for indolene. It builds on a study[6] that showed the efficacy of the base case configuration of fuel droplet combustion shown in Figure 2 to assess the extent to which several hydrocarbons often considered as surrogates for gasoline in fact reproduced its combustion performance.

We employ the droplet configuration of Figure 2 to study the combustion of indolene. The relevance of droplets to the broader context of engines is that droplets represent the fine grid structure of sprays. The single isolated droplet is the base case for liquid fuel combustion through the simplified transport that characterizes it, as well as the phase equilibrium and moving boundary effects promoted by heat transfer to the droplet and evaporation at the droplet surface. The baseline configuration consists of a droplet, a soot shell,[27] and a flame all concentric to one another. The streamlines of the flow (shown in Figure 2 as dotted lines with arrows) are purely radial.

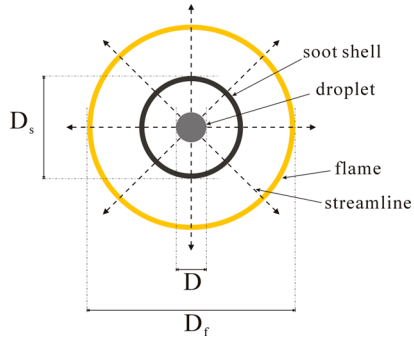

Figure 2. Schematic of a spherically symmetric droplet flame.

The present study provides the first examination of the detailed droplet burning behavior of indolene and compares results with a commercial grade gasoline. The combustion properties compared between indolene and gasoline are (cf. Figure 2) the size evolutions of the droplet (D), soot shell (D_s), and flame (D_f).

For fuels such as indolene and gasoline with a significant aromatic content, soot formation will be a prominent feature of the droplet burning process. Soot forms between the droplet and flame (on the fuel-rich side of diffusion flames) when the forces acting on the soot aggregates balance.[27−29] It is noted that the mechanisms for establishing the soot shell—the thermophoretic and evaporation-induced forces—are relevant to the engine environment, even if the spherical geometry shown in Figure 2 is never realized in an engine. The configuration of Figure 2 should be viewed for the simplicity that it brings to the droplet burning process while still including evaporation, phase equilibrium, and particulate emissions for a transport dynamic that is eminently modelable.

In the present study, fuel droplets with initial diameters of approximately 0.53 mm are ignited and burned in air at atmospheric pressure. In the following, Section 2 describes the experimental details and Section 3 discusses the results.

dx.doi.org/10.1021/ef3007849 | *Energy Fuels* 2012, 26, 5740−5749

2. EXPERIMENTAL METHODS

2.1. Apparatus. The experiments are carried out in a facility that reduces the effects of convection in order to promote spherical symmetry of the droplet burning process (cf. Figure 2). The experimental design and procedures follow the description given in ref 6 where further details can be found. A brief description is given here.

Spherical droplet flames are promoted by burning test droplets in a stagnant ambience, restricting their motion by mounting them onto very small (14 μm diameter SiC) fibers and carrying out the experiments in a low gravity environment. The totality of these conditions produces low Reynolds and Rayleigh numbers, the combination of which promotes spherical gas phase symmetry in the droplet burning process. Low gravity, on the order of 10^{-4} of the Earth's normal gravity, is created by doing the experiments in a free-fall facility that incorporates a drag shield. Droplets with initial diameters ranging from 0.47 mm to 0.59 mm with an average of 0.53 $\pm$ 0.05 mm were examined.

Droplets of such initial diameters are large enough that a significant fraction of their burning history could be accurately recorded, and they are not too small that there would be issues with optically resolving them and compromising data quality.

The fiber support structures are placed in a crossing pattern with the test droplets deployed at the intersection of the fibers. In this way, droplets do not slide along the fiber as they burn. The temperature field surrounding the droplet will also be more symmetrical compared to a droplet placed at the end of a single support fiber,[30] which significantly distorts the soot patterns. Droplets are ignited by sparks established across two electrode pairs positioned on opposite sides of the droplet, and the burning history is recorded by two cameras to document the evolution of the droplet and sooting dynamics and the flame. Once ignited, the electrodes are rapidly retracted. A color video camera records self-illuminated flame images (at 0.3 MP per frame using a Hitachi HV-C20 camera operated at 30 frames per second, and fitted with a Nikkor 135 mm f/2.0 lens and two Kenko 36 mm extension tubes); a black and white (BW) digital high-speed camera is used to obtain backlit images (a 3.9MP per frame Canadian Photonics Laboratories, Inc. MS-80K digital high speed camera operated at 200 fps with an Olympus Zuiko 90 mm f/2.0 lens, an Olympus OM Telescopic Extension Tube 65−116 mm (fixed at 100 mm), and a Vivitar MC 2X teleconverter) that facilitate recording droplet and soot shell boundaries. A 1-W LED lamp (Black Diamond) is used for backlighting. Some representative visualizations from this optical arrangement are shown in Figure 3 and discussed in Section 3.

It has previously been shown that the support fibers used here have a minimal effect on the overall burning process.[6,31−33] The fiber can influence the burning process by heat conduction through the fiber due to the temperature difference between the fiber and surrounding gas, the sooting configuration by altering the symmetry of the temperature distribution in the gas phase surrounding the droplet, and the soot structure and flame shape by providing a surface on which soot aggregates can stick. The idealized configuration of Figure 2 assumes that the flow field created by the evaporation process is in the purely radial direction so that a spherical soot pattern would form at a location where the forces on the soot aggregates balance.[27]

Simplified models of heat transfer through a fiber[32] have examined the influence of the fiber and its properties on the burning rate, K. On the experimental side, the influence of a support fiber[32] on the configurations produced by soot aggregates being trapped between the droplet and flame was experimentally examined.[30] Comparisons have been reported on the evolution of droplet diameter for fibers of different thermal conductivities[6] and between free-floating and fiber-supported droplets.[33] The results suggest that, for the conditions of the present study, the droplet burning rate should not be significantly influenced by the fiber. However, the photographic evidence does show that the shape of the soot "shell" and aggregation of soot particles may be influenced by the fiber, even for the small fiber sizes employed in the present study. Fibers as small as 7 μm with $D_o \sim 0.6$ mm were still found to influence the soot shell configurations.[34] Nonetheless, the distortions of the soot shell associated with aggregates being attached to the fiber were not considered to exert a determinative influence on the droplet burning rate for the present study, as noted in Section 3.

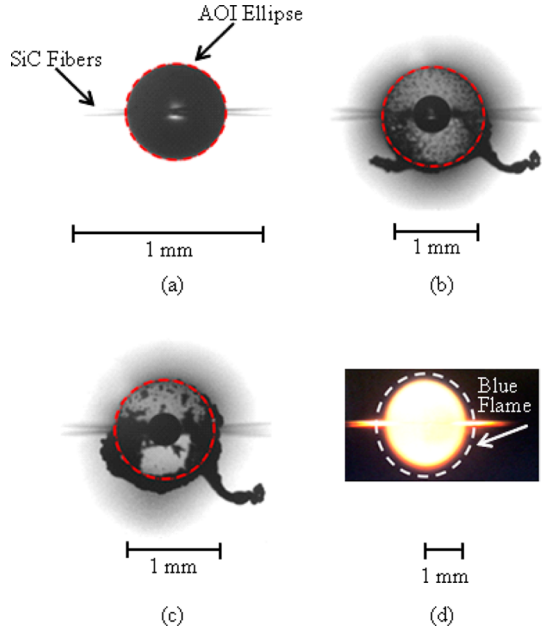

Figure 3. Illustration of dimension measurements for droplet diameters (a), soot shell diameters (b), soot shell diameters when only a partial shell is visible (c) from BW images, and flame diameters (d) from color images.

2.2. Image Analysis. The main diagnostic of this study employs cameras and frame analysis to extract quantitative data. The analysis software used to measure droplet and soot shell diameters (Figure 2) was Image-Pro Plus v6.3 (Bethesda, MD). The analysis involves placing an area of interest (AOI) ellipse on top of the droplet or soot shell in the black and white (BW) images. An AOI is also fitted to a calibration ball bearing to obtain a conversion factor between pixels and millimeters. The calibration bearing (a 0.79 mm tungsten carbide ball) is also recorded at the same lighting conditions as were the fuel droplets.

Examples of AOIs that show the droplet and soot structure are shown in Figure 3, parts a and b, respectively; Figure 3d shows the flame, which is spherical, as expected. Determining an AOI for the soot shell becomes inherently more difficult due to agglomeration of the soot particles during burning. Because of this effect, there will be periods when the soot shell is only partially visible. In this study, a partially visible soot shell is considered valid for measurement if at least two arcs of the soot shell are visible from which an ellipse can be fitted. For indolene droplets, examples of the AOI determined for a complete and a partially visible soot shell are shown in Figure 3, parts b and c, respectively.

The flame diameter was measured using CorelDraw 9. An ellipse tool was used to outline the outer luminous zone of the droplet flame, as shown in Figure 3d. The flame boundary is taken as the outer edge of the blue section of the flame which surrounds the inner yellow core (due to soot oxidation). This can be seen in Figure 3d. The 0.79 mm tungsten carbide ball bearing is also analyzed using the CorelDraw 9 software to establish a conversion factor needed to obtain the flame diameter in millimeters.

2.3. Fuels. The indolene comes from Haltermann Solutions (Houston, TX, Federal Certification Fuel EPA TIER II EEE, HF437).[3] The gasoline used in the experiments was an 87 octane rated unleaded gasoline with no ethanol. It was purchased from a local Mobil station in Ithaca, NY, in November 2009. Selected properties for indolene and gasoline are listed in Table 1. Densities of indolene from 15 to 27 °C are shown in Figure 4. This range is based on the specifications and restrictions of the digital density meter used for the measurements (i.e., a Mettler-Toledo DA-100 M density meter).

3. RESULTS AND DISCUSSION

3.1. Qualitative Observations. Figure 5 shows the evolution of flame images at 0.1 s intervals for gasoline and

dx.doi.org/10.1021/ef3007849 | Energy Fuels 2012, 26, 5740−5749

Table 1. Selected Properties of Indolene and Gasoline

	indolene	gasoline (87 octane)
formula	$C_{9.97}H_{18.42}$ [a]	$C_{8.26}H_{15.50}$ [b]
stoichiometric air/fuel ratio ν [c]	14.578	12.135
H/C ratio [d]	1.847	1.877
molecular weight, W (g/mol) [e]	138.3	114.8
B.P. (K)	303−474 [f]	297−494 [g]
liquid density, ρ_L (kg/m^3) [h]	739	731
antiknocking index [i]	92.75	87
quasi-steady burning rate, K (mm^2/s) [j]	0.57	0.53

[a]Calculated from the carbon and hydrogen ratio and carbon weight percent in ref 3. [b]Obtained from ref 36. [c]$\nu = n + m/4$, where n and m come from the formula C_nH_m. [d]H/C ratio = m/n, where n and m come from the formula C_nH_m. [e]Calculated from the formula. [f]Ref 3. [g]Ref 38. [h]Measured using a digital density meter (Mettler Toledo DA-100M) at 297.7 K. [i]Antiknocking index (AKI) = (research octane number (RON) + motor octane number (MON))/2. [j]Estimated using the method pertaining to the fourth order polynomial provided and discussed in Appendix A.

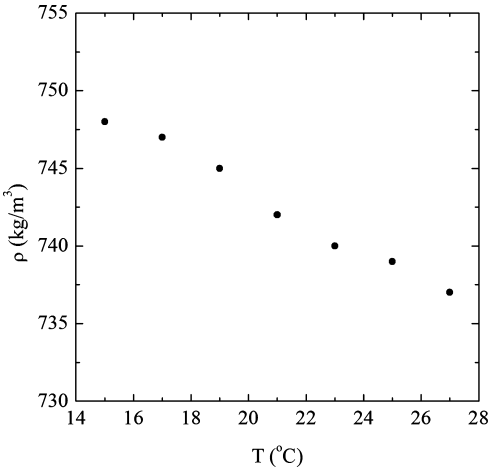

Figure 4. Density measurements for indolene at T = 15 to 27 °C.

indolene droplets. The nearly spherical flames indicate that convection effects were reduced by burning the droplets in a low gravity environment while anchored to the SiC support fibers. The glowing protrusions seen on either side of the flames are a result of the interaction between the flames and SiC fibers.

As shown in Figure 5, the flames are slightly elongated vertically, though the distortion is not especially pronounced. This effect can evidence motion of soot aggregates being restricted by the fiber, while in the vertical direction they will be free-floating. As the flame luminosity is due to oxidation of soot, the soot and luminous zone are able to move more freely without a fiber influence, while in the horizontal direction the motion of the luminous zone is more restricted because aggregates cannot move as freely. This effect appears to result in a slightly nonspherical flame (luminous zone).

Also evident in Figure 5 is that indolene flames appear larger and brighter than gasoline flames for similar initial droplet sizes. The flame brightness of the indolene flames persists for a longer period compared to gasoline flames owing to a longer period of soot oxidation.

Flame brightness provides a qualitative measure of the sooting propensity of fuels due to sensitivity of the eye to wavelengths in the visible region of the spectrum. On this basis, Figure 5 would suggest that the brighter indolene flames have

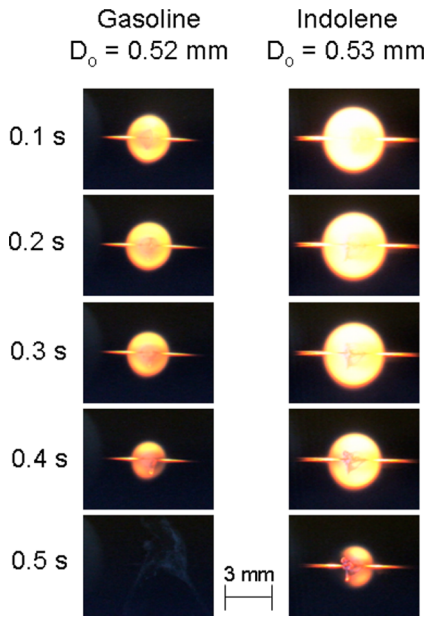

Figure 5. Color images showing the evolution of spherical droplet flames for indolene and gasoline droplets.

more soot formation compared to gasoline. This general trend is consistent with the backlit images shown in Figure 6.

The series of photographs shown in Figure 6 show the evolution of soot formation around gasoline and indolene droplets of similar initial droplet diameter. The soot shells are clearly visible and reside between the droplet and flame as expected (for the backlit image, the flame is not visible in the sequence of Figure 6, as it will be well outside the sooting zone). Indolene droplets tend to form thicker soot shells than gasoline droplets in the early stages of burning. Along with the qualitative results of Figure 5, the soot shell images in Figure 6 suggest that indolene is more sooting than gasoline.

The reason for differences in the sooting tendencies of gasoline and indolene is unclear, and hypotheses grounded in the qualitative nature of the experimental results presented in this study (i.e., Figures 5 and 6) cannot offer definitive interpretations. Our speculation is that differing aromatic content in the fuels could be responsible for the differing sooting tendencies observed. The indolene examined in the present study had an aromatic (volume) concentration of 28%.[3] For the gasoline examined in this study, and given the time of year it was purchased, the aromatic content should be about 24%.[35] The slightly brighter indolene flames would be consistent with the slightly higher aromatic content of indolene compared to gasoline.

3.2. Quantitative Comparisons. A quantitative comparison between the droplet, soot, and flame dynamics of gasoline and indolene is shown in Figure 7. Measurements of the droplet diameters are shown using classical scaling from the D^2 law,[36]

$$\left(\frac{D}{D_o}\right)^2 = 1 - K\left(\frac{t}{D_o^2}\right) \quad (1)$$

The gasoline data shown in Figure 7 are an average of three runs[6] and the indolene data are comprised of four separate runs. The initial fluctuations seen in the indolene data are from one run (D_o = 0.59 mm) during which the spark energy deformed the droplet at the onset of burning. Data within the first 0.2 s/mm^2 in this run are affected by this droplet deformation. However, this initial disturbance did not affect the remainder of burning, and the other three indolene runs do not have this initial disturbance from the spark.

dx.doi.org/10.1021/ef3007849 | Energy Fuels 2012, 26, 5740−5749

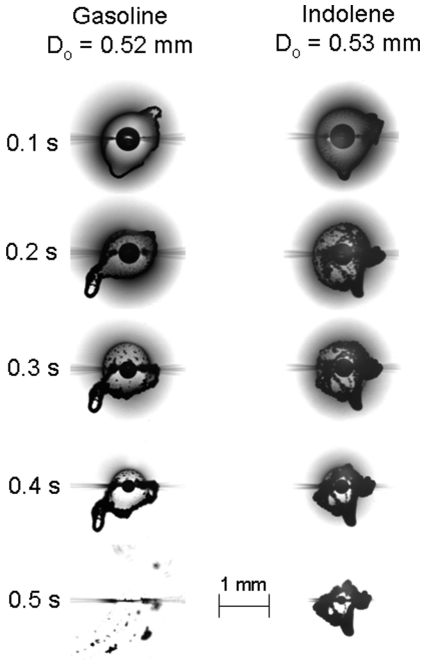

Figure 6. Backlit BW images showing the evolution of droplet size and soot shell dynamics for indolene and gasoline droplets.

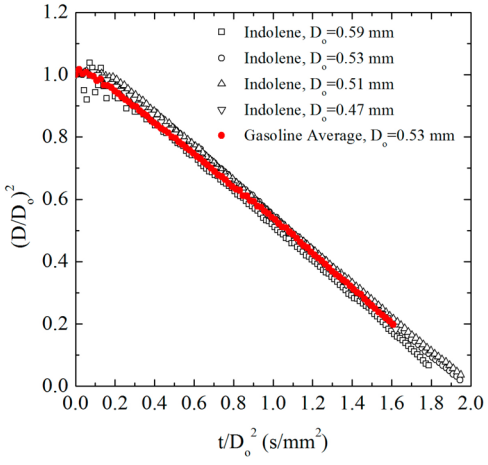

Figure 7. Evolution of droplet diameters for indolene droplet combustion (black open symbols) compared with the averaged gasoline data from ref 6 (red data).

It is clear that the evolution of droplet diameter for gasoline and indolene shown in Figure 7 is remarkably similar. Figure 8 shows the averaged data that was computed by averaging the individual data of Figure 7 at each specific time. The gap in the indolene data at the end (cf. Figure 8) is due to the averaging process among the data sets. The overall trend is the same for both fuels, which is more easily seen by considering just the average data shown in Figure 8. The data show that indolene is an excellent match for gasoline over the range 0.5 s/mm^2 $\leq t/D_o^2 \leq$ 1 s/mm^2, with slight deviations occurring at the beginning and end of burning.

A sixth order polynomial is fitted to the averaged data shown in Figure 8 to give the evolution of burning rate, K (the derivative of the fit), shown in Figure 9. Appendix A discusses the impact of using various orders of polynomials on analyzing this type of data. The evolutions of K for indolene and gasoline are nearly identical, thus indicating that both fuels evaporate at almost the same rate during the combustion process. During the early stages of burning,

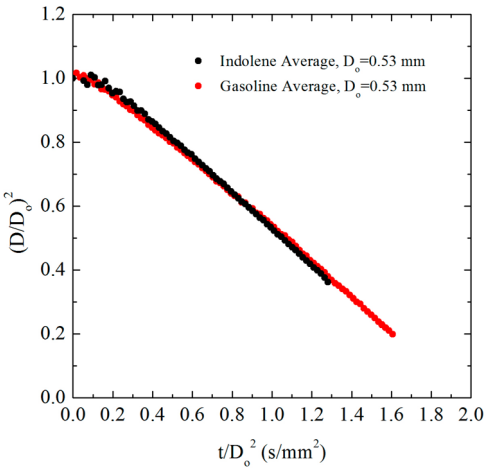

Figure 8. Comparison of averaged droplet size evolution for indolene (black data) and gasoline (red data[6]).

indolene appears to have a slightly lower burning rate compared to gasoline, though in fact the burning rates may be considered to be virtually identical within the precision of the data analysis process and photographic quality of the burning history that was recorded in the present investigation. A quasi-steady period is seen for 0.5 s/mm^2 $\leq t/D_o^2 \leq$ 1 s/mm^2, as noted, where $K_{indolene} \sim K_{gasoline}$. The final slight increase in burning rate shown in Figure 9 for indolene is most likely an artifact of the sixth order polynomial fit of the data in Figure 8 (see Appendix A for more details).

According to the classical D^2 law, the quasi-steady burning rate is proportional to properties as[6,36]

$$K \propto \frac{k_g/c_{p,g}}{\rho_L} \tag{2}$$

The compositions of indolene and gasoline include hydrocarbon components (cf. Figure 1) that have thermal properties that are not substantially different. According to eq 2, the most important liquid property is density. Since the densities of gasoline and indolene are close, similar burning rates will be expected, which is consistent with Figure 9.

The evolutions of flame and soot shell diameters are shown in Figures 10 and 11, respectively. The flame and soot stand-off ratios (FSR and SSR), defined as D_f/D and D_s/D, respectively, are instantaneous measures of how far the flame and soot shells are positioned from the droplets. Broadly noted, $D_s/D < D_f/D$ is a consequence of soot forming on the fuel rich side of the flame.[27,28] As shown in Figures 10 and 11, indolene produces flames that are farther away from the droplet compared to gasoline droplet flames, which is consistent with Figure 5, as discussed previously.

The classical theory of FSR as extended by Aharon and Shaw[37] results in relative flame positions, $\Theta \equiv (FSR_{indolene})/(FSR_{gasoline})$, as[6]

$$\Theta \equiv \frac{FSR_{indolene}}{FSR_{gasoline}} \approx \left(\frac{\rho_{L,indolene}}{\rho_{L,gasoline}}\right)\left(\frac{K_{indolene}}{K_{gasoline}}\right)\left(\frac{\nu_{indolene}}{\nu_{gasoline}}\right)\left(\frac{W_{gasoline}}{W_{indolene}}\right) \tag{3}$$

With values of ρ_L, K, ν, and W for both indolene and gasoline from Table 1, we find that $\Theta \sim 1.08$. This result suggests that indolene should have a slightly higher FSR than gasoline, which is consistent with Figure 10, though the differences in Figure 10 are much larger. This may be due to the approximate nature of the theory or uncertainties in estimating the variables for eq 3.

The SSR for indolene and gasoline are compared in Figure 11. During the early stages of burning, indolene produces soot shells

dx.doi.org/10.1021/ef3007849 | Energy Fuels 2012, 26, 5740−5749

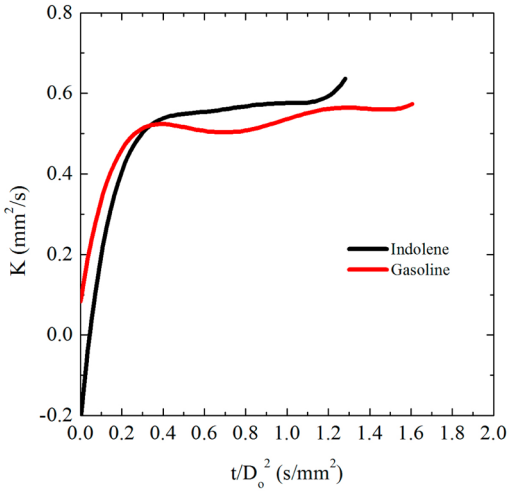

Figure 9. Burning rate curves obtained from the first derivative of a sixth order polynomial fitted to indolene and gasoline[6] data.

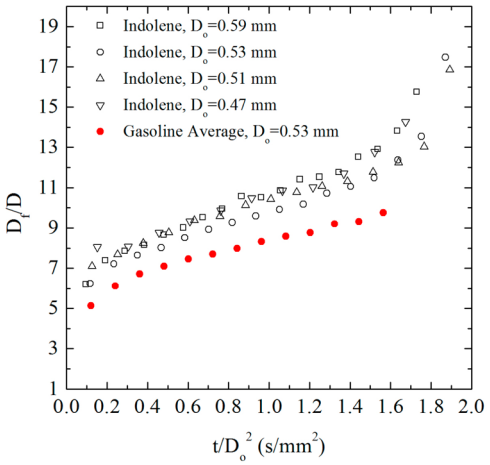

Figure 10. Evolution of flame standoff ratio (FSR, D_f/D) for four runs of indolene compared with averaged gasoline data.[6]

that are comparatively farther from the droplet surface than gasoline soot shells. At approximately t/D_o^2 = 1.1 s/mm^2, the SSRs for the two fuels are equivalent. After this period, the soot shell produced by the indolene droplet is closer to the droplet than the soot shell produced by the gasoline droplet. This is also seen in Figure 6: between 0.1 and 0.3 s, the soot shell surrounding the indolene droplet seems to be noticeably farther from the droplet than the soot shell for the gasoline droplet. However, after this point in time, the soot shell around the indolene droplet is closer to the droplet, whereas the soot shell surrounding the gasoline droplet does not show this behavior.

It is interesting that the range of chemical compositions that comprise gasoline and indolene (Figure 1), which might be expected to produce differing droplet burning characteristics, do not greatly affect all of the indolene and gasoline droplet combustion characteristics. Certainly, the evidence shows that the burning rates (Figures 7−9) are not influenced by these compositional differences. However, the FSR and SSR data shown in Figures 10 and 11 show differences that cannot be explained solely on the basis of experimental uncertainty. The FSR is influenced by soot formation (through oxidation of the soot). A definitive explanation of the sooting characteristics of gasoline and indolene droplet flames awaits a more complete examination of soot formed in droplet flames.

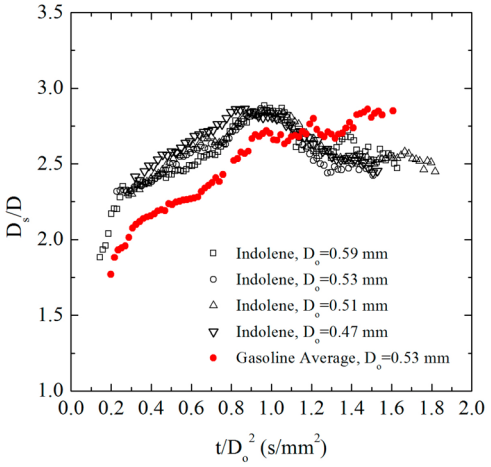

Figure 11. Comparison of soot standoff ratio (SSR, D_s/D) for indolene and gasoline.[6]

4. CONCLUSIONS

Data are reported for the base case of droplet combustion with spherical symmetry for gasoline and indolene. Results show that some aspects of the combustion process are remarkably similar between the two fuels, while others are different: (1) the evolution of droplet diameter (squared) and burning rate of indolene are very close to the commercial grade gasoline employed in the experiments; (2) indolene flames reside farther from the droplet surface than the flames surrounding gasoline droplets for similar initial droplet diameters; and (3) indolene droplets have a slightly different soot shell dynamic than gasoline droplets, with the soot shell of indolene droplets being comparatively farther from the droplet initially, then drawing closer to the droplet surface near the end of burning. As a final note, the configuration of spherically symmetric droplet burning is a useful canonical configuration to examine and compare the combustion characteristics of practical fuels.

APPENDIX A: DISCUSSION ON VARIOUS ORDERS OF POLYNOMIAL FITS TO D^2 DATA

This section examines the influence of processing data such as those shown in Figure 8 on determining the burning rate from

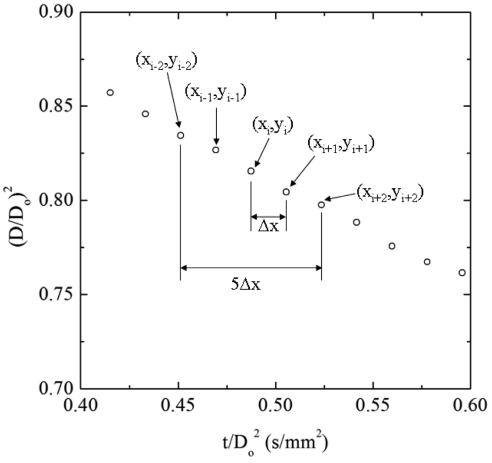

Figure A1. A portion of droplet size data for indolene (black data in Figure 8) that is used to illustrate how two-point difference methods are executed to obtain local burning rates using different spacing (Δx and $5\Delta x$) for the slopes.

dx.doi.org/10.1021/ef3007849 | Energy Fuels 2012, 26, 5740−5749

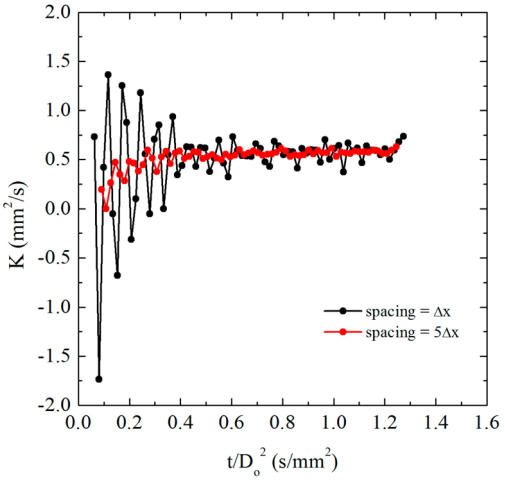

Figure A2. Computed local burning rates using space Δx and $5\Delta x$ for the two-point difference method.

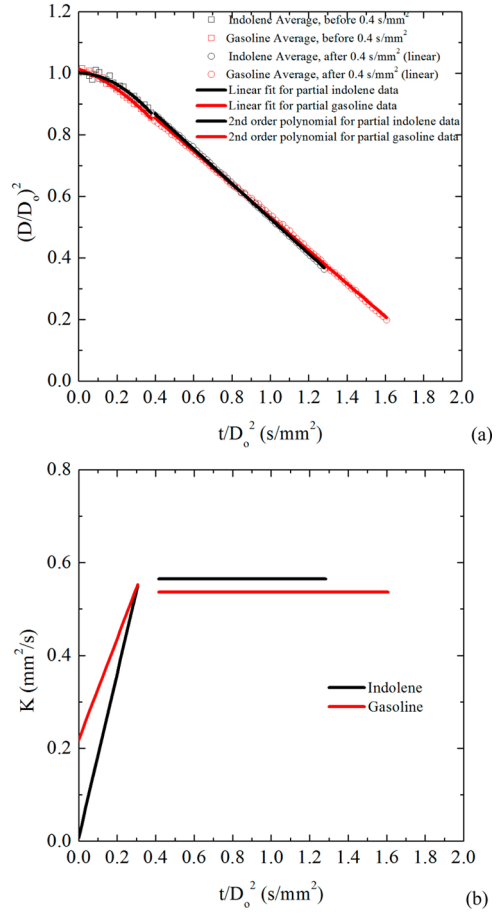

Figure A3. (a) Droplet size data from Figure 8 for indolene and gasoline fitted with a second order polynomial for the transient region (t/D_o^2 = 0–0.4 s/mm^2) and a linear fit for the quasi-steady region (t/D_o^2 > 0.4 s/mm^2); (b) the burning rates calculated using the fits in a.

data. Approaches considered are akin to finite differencing the data and imposing polynomial fits of various orders on the measurements.

Differentiating the data in a way analogous to a finite difference estimate of a derivative (Figure A1) leads to the

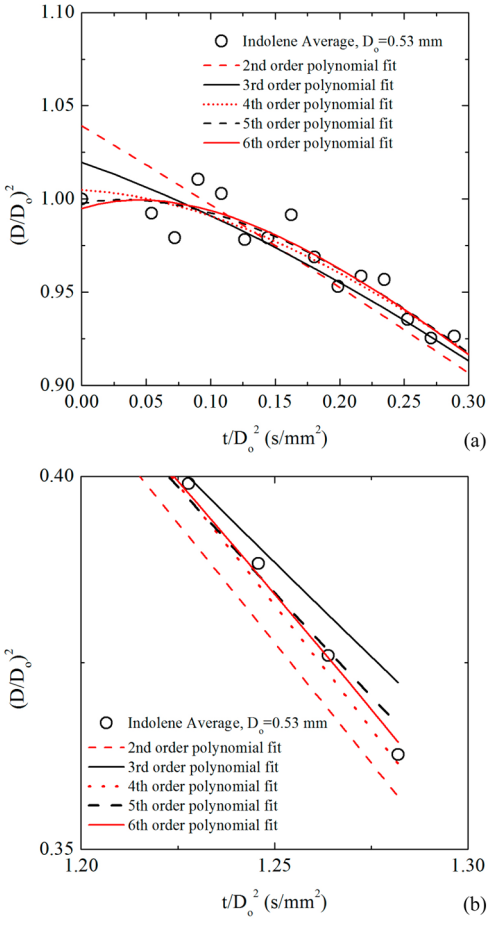

Figure A4. Various orders of polynomials fitted on the average droplet size data for indolene (black data in Figure 8): enlargement of the beginning of burning (a) and the end of burning (b).

following expression for the burning rate:

$$K_{i,\Delta x} = -\frac{(y_{i+1} - y_i)}{(x_{i+1} - x_i)} = -\frac{(y_{i+1} - y_i)}{\Delta x} \tag{A1}$$

This burning rate is assigned a time,

$$(t/D_o^2)_{i,\Delta x} = \frac{x_{i+1} + x_i}{2} \tag{A2}$$

The burning rates calculated in this fashion are shown by the black data in Figure A2. The resulting burning rates fluctuate significantly. This approach amplifies the physical impact of sparks on the droplet earlier in the burning and the slight error produced by manual measurements for the droplet size. The reason the error becomes so obvious is that the time interval between each data point is very small so that K becomes sensitive to the D^2 data.

A larger time spacing (e.g., $5\Delta x$) could be used to alleviate this problem,

$$K_{i,5\Delta x} = -\frac{y_{i+2} - y_{i-2}}{x_{i+2} - x_{i-2}} = -\frac{y_{i+2} - y_{i-2}}{5\Delta x} \tag{A3}$$

for the time

$$(t/D_o^2)_{i,5\Delta x} = x_i \tag{A4}$$

The red data in Figure A2 show the results. The fluctuation is reduced and the quasi-steady (t/D_o^2 = 0.4–1.0 s/mm^2) burning

dx.doi.org/10.1021/ef3007849 | Energy Fuels 2012, 26, 5740–5749

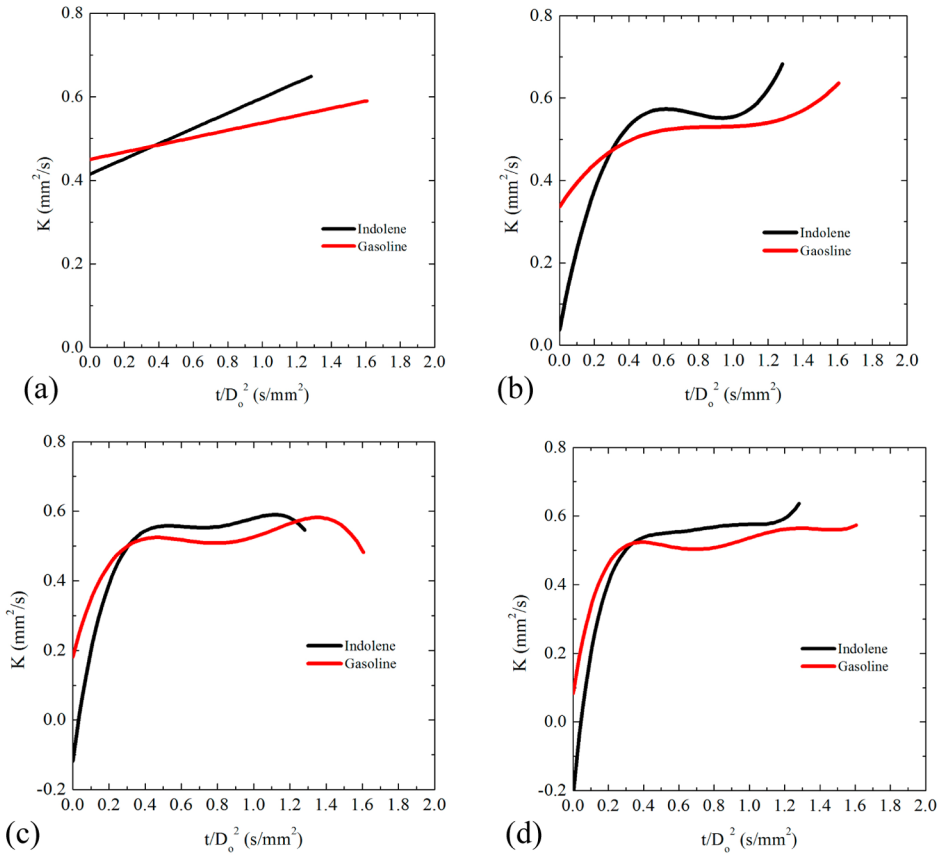

Figure A5. Burning rate curves calculated for droplet size data from Figure 8 by fitting secnd (a), fourth (b), fifth (c), and sixth (d) order polynomial for indolene and gasoline.

Table AI. Comparison of the Calculated Burning Rates Obtained from Various Fitting Methods[a]

	quasi-steady burning rate, K (mm^2/s)	
	indolene (D_o = 0.53 mm)	gasoline (D_o = 0.53 mm)
linear	0.565	0.536
2nd order polynomial	0.532	0.520
4th order polynomial	0.565	0.531
	(0.56−0.90 s/mm^2)	(0.63−1.19 s/mm^2)
5th order polynomial	0.563	0.536
	(0.51−1.08 s/mm^2)	(0.51−1.41 s/mm^2)
6th order polynomial	0.561	0.534
	(0.42−0.99 s/mm^2)	(0.42−1.50 s/mm^2)

[a]Values in parentheses show the range of t/D_o^2 (s/mm^2) from which the quasi-steady values are computed. The burning rate value for linear fit is from the direct derivative of the linear fit; the value for the second order polynomial is computed by averaging the data in the entire burning.

rate does not change much compared to using a smaller time interval (black, K = 0.561 mm^2/s; red, K = 0.564 mm^2/s).

Since the evolution of scaled droplet diameter included in Figure 8 appears to be nearly linear, a linear fit to the data may be a reasonable approximation. Figure A3a shows such linear fits for indolene and gasoline for the quasi-steady region (t/D_o^2 > 0.4 s/mm^2) in Figure 8. For the transient heating region (t/D_o^2 < 0.4 s/mm^2) a second order polynomial is used to capture the local curvature. The burning rates calculated from the derivatives of the linear and second order polynomial fits for indolene and gasoline are shown in Figure A3b. Though a lower order of fitting is used in this case, this approach is still able to capture some characteristics of burning, that is, gasoline's higher burning rate in the transient region and lower burning rate in the quasi-steady stae compared to that of indolene.

Figure A4a shows the efficacy of various orders of polynomials in representing the $(D/D_o)^2$ data with more nonlinearity in the transient heating region of indolene droplet burning, t/D_o^2 < 0.3 s/mm^2. With higher order polynomials, the curvature from 0 to 0.15 s/mm^2 is gradually improved. Both fifth and sixth order polynomials undershoot the initial diameter ($(D/D_o)^2$ = 1.0), but the fifth order fit has the closest initial value among all fits.

Figure A4b shows polynomial fits for indolene at t/D_o^2 > 1.22 s/mm^2. In this region, polynomials with an even order tend to undershoot the data whereas odd order polynomials overshoot the data. This might be due to the difference in concavity between even and odd order polynomials. Nonetheless, it is still evident that a polynomial with a higher order better fits the data in a local sense.

Figure A5 compares the burning rate curves computed using various order polynomial fits, second (a), fourth (b), fifth (c), and sixth (d), for indolene and gasoline. It is clear that a second order fit does not capture the transient variations (Figure A5a). Figure A4b shows that the K determined from a fourth order fit captures more details of the burning rate than does the second order fit. Nonetheless, the drawback of using only one polynomial to fit the entire D^2 data is that the fitted curve will sacrifice the linearity of the data at larger t/D_o^2 in order to accommodate the data at smaller t/D_o^2. This leads to an

dx.doi.org/10.1021/ef3007849 | Energy Fuels 2012, 26, 5740−5749

increase in calculated burning rates at t/D_o^2 =1.4 s/mm^2 (see Figure A5b), which is an artifact resulting from the use of this particular polynomial.

Burning rates calculated using fifth and sixth order polynomials for indolene and gasoline are shown in Figure A5, parts c and d, respectively. It is evident that the higher order polynomial fits are more sensitive to the local evolution of $(D/D_o)^2$. The quasi-steady plateau for the fifth and sixth order fits is realized at $t/D_o^2 \sim 0.4$ s/mm^2 (compared to about 0.5 s/mm^2 for the fourth order fits). Interestingly, the increase of the burning rate after the quasi-steady region seen in the fourth order burning rate curves no longer exists in either the fifth or sixth order burning rate curves. However, a higher order polynomial such as a sixth order fit is more greatly affected by the local fluctuations of $(D/D_o)^2$. It is worth noting that the fifth order burning rates decrease at the end, whereas the fourth and sixth order fits behave in the opposite way. This appears to be caused by the intrinsic concavity of the polynomial and thus does not reflect the real burning rates.

Table AI compares the quasi-steady burning rates obtained from four polynomials shown in Figure A5 for indolene and gasoline. Surprisingly, regardless of how accurate a higher order polynomial is able to capture the local variation of data, all of these methods provide very similar quasi-steady burning rates for indolene and gasoline.

AUTHOR INFORMATION

Corresponding Author

*Email: yl677@cornell.edu.

Notes

The authors declare no competing financial interest.

ACKNOWLEDGMENTS

The authors thank Michael Hicks of the National Aeronautics and Space Administration for serving as project monitor (through NASA grant number NNX08AI51G) and for helpful discussions and suggestions. The authors also acknowledge fruitful discussions with Brad Zigler of the National Renewable Energy Laboratory who also supplied the indolene used in this study, and Kevin Stork of the U.S. Department of Energy.

NOMENCLATURE

c_p = specific heat (J/g·K)
D = diameter (if no subscripts, droplet diameter) (mm)
K = burning rate ($\equiv -d(D/D_o)^2/d(t/D_o^2)$, mm^2/s)
k = thermal conductivity (W/m·K)
T = temperature (K or °C)
t = time (s)
W = molecular weight (g/mol)
x = quantity of t/D_o^2 in a D^2 plot in Appendix A (s/mm^2)
y = quantity of $(D/D_o)^2$ in a D^2 plot in Appendix A

Greek Letters:

ν = stoichiometric ratio
Θ = defined parameter in eq 3
ρ = density (kg/m^3)

Subscripts:

f = flame
g = gas or vapor state
i = the i^{th} data point along the D^2 plot in Appendix A
L = liquid state
o = initial value
s = soot shell

REFERENCES

(1) Johnson, R. T.; Riley, R. K.; Feasibility of Methanol/Gasoline Blends for Automotive Use. In *Evaporation−Combustion of Fuels*, Advances in Chemistry Series; American Chemical Society: Washington, DC, 1978; pp 245−266.

(2) United States Patent and Trademark Office, Trademark Serial number: 71225514, Mark: Indolene, 1926. http://assignments.uspto.gov/assignments/q?db=tm&sno=71225514

(3) *Product Information of EPA TIER II EEE Federal Register HF437*; Haltermann Solutions, Houston, TX, 2010.

(4) *Specification of UTG 96*; Chevron Phillips Chemical Company LP, The Woodlands, TX, 2008.

(5) Cromas, J. Particulate Matter Formation Mechanisms in a Direct-Injection Gasoline Engine. Master's Thesis, Mechanical Engineering, University of Wisconsin-Madison, 2003.

(6) Liu, Y. C.; Avedisian, C. T. *Combust. Flame* **2012**, *159*, 770−783.

(7) Manufacturers of Emission Controls Association. *The Impact of Gasoline Fuel Sulfur on Catalytic Emission Control Systems*; manufacturers of Emission Controls Association: Washington, DC, Sept. 1998; available online: http://www.meca.org/galleries/default-file/sulfur.pdf.

(8) Bykowski, B. B.; Garbe, R. J. *Ind. Eng. Chem. Prod. Res. Dev.* **1981**, *20*, 726−734.

(9) Kayes, D.; Hochgreb, S. *Environ. Sci. Technol.* **1999**, *33*, 3968−3977.

(10) Dimou, I. Particulate Matter Emissions from a DISI Engine under Cold-Fast-Idle Conditions for Ethanol−Gasoline Blends. Master Thesis, Mechanical Engineering and Naval Engineer at the Massachusetts Institute of Technology, 2011

(11) Hibert, D. *High Ethanol Fuel Endurance: A Study of the Effects of Running Gasoline with 15% Ethanol Concentration in Current Prodction Outboard Four-Stroke Engines and Conventional Two-Stroke Outboard Marine Engines*, NREL/SR-5400-52909; National Renewable Energy Laboratory: Golden, CO, 2011.

(12) Kar, K.; Cheng, W. Using Mass Spectrometry to Detect Ethanol and Acetaldehyde Emissions from a Direct Injection Spark Ignition Engine Operating on Ethanol/Gasoline Blends. SAE Technical Paper 2011-01-1159, 2011.

(13) Daw, C. S.; Edwards, K. D.; Wagner, R. M.; Green, J. B., Jr. *J. Eng. Gas Turbines Power* **2008**, *130*, 052801.

(14) Farrel, J. T.; Bunting, B. G. Fuel Composition Effects at Constant RON and MON in an HCCI Engine Operated with Negative Valve Overlap. SAE Technical Paper 2006-01-3275, 2006.

(15) Zigler, B. T.; Walton, S. M.; Assanis, D.; Perez, E.; Wooldridge, M. S.; Wooldridge, S. T. *J. Eng. Gas Turbines Power* **2008**, *130*, 052803.

(16) Andesen, V. F.; Anderson, J. E.; Wallington, T. J.; Mueller, S. A.; Nielsen, O. J. *Energy Fuels* **2010**, *24*, 2683−2691.

(17) Andersen, V. F.; Anderson, J. E.; Wallington, T. J.; Mueller, S. A.; Nielsen, O. J. *Energy Fuels* **2010**, *24*, 3647−3654.

(18) Metghalchi, M.; Keck, J. C. *Combust. Flame* **1982**, *48*, 191−210.

(19) Abu-Isa, I. A. *Rubber Chem. Technol.* **1983**, *56* (1), 169−196.

(20) Ganley, J. T.; Springer, G. S. *Environ. Sci. Technol.* **1974**, *8* (4), 340−347.

(21) Gauthier, B. M.; Davidson, D. F.; Hanson, R. K. *Combust. Flame* **2004**, *139*, 300−311.

(22) Yahyaoui, M.; Djebaïli-Chaumeix, N.; Dagaut, P.; Paillard, C.-E.; Gail, S. *Proc. Combust. Inst.* **2007**, *31*, 385−391.

(23) Choi, B. C.; Choi, S. K.; Chung, S. H. *Proc. Combust. Inst.* **2011**, *33*, 609−616.

(24) Bieleveld, T.; Frassoldati, A.; Cuoci, A.; Faravelli, T.; Ranzi, E.; Niemann, U.; Seshadri, K. *Proc. Combust. Inst.* **2009**, *32*, 493−500.

(25) Dagaut, P.; Togbé, C. *Fuel* **2008**, *87*, 3313−3321.

(26) Chaos, M.; Zhao, Z.; Kazakov, A.; Gokulakrishnan, P.; Angioletti, M.; Dryer, F. L. A PRF+Toluene Surrogate Fuel Model for Simulating Gasoline Kinetics. *The 5th U.S. Combustion Meeting*, San Diego, CA, March 25−28, 2007.

(27) Avedisian, C. T.; *Physical and Chemical Aspects of Combustion*; Amsterdam B.V. Published under license by Gordon and Breach Science Publishers: Amsterdam, 1997; pp 135−160.

(28) Jackson, G. S.; Avedisian, C. T.; Yang, J. C. *Int. J. Heat Mass Transfer* **1992**, *35* (8), 2017−2033.
(29) Jackson, G. C.; Avedisian, C. T. *Combust. Sci. Technol.* **1996**, *115*, 125−149.
(30) Avedisian, C. T.; Jackson, G. S. *J. Prop. Power* **2000**, *16*, 974−979.
(31) Bae, J. H.; Avedisian, C. T. *Combust. Flame* **2004**, *137*, 148−162.
(32) Tanvir, F.; Dryer, F. L. *Combust. Flame* **2012**, *159*, 200−209.
(33) Callahan, B. J. Droplet Combustion of Nonane, Hexanol, and Their Mixtures in Reduced Gravity. Master Thesis, Mechanical and Aerospace Engineering, Cornell University, Ithaca, NY, 2000.
(34) Pan, K. L.; Li, J. W.; Wang, C. H. *Combust. Flame* **2009**, *156*, 1926−1936.
(35) The Energy Future Coalition. *Comments on The Environmental Protection Agency's Proposed Rule: Control of HaardousAir Pollutants from Mobile Sources*, EPA-HQ-OAR-2005-0036, 70 Fed Reg. 15804; The Energy Future Coalition: Washington, DC, 2006.
(36) Turns, S. R. *An Introduction to Combustion-Concepts and Applications*, 2nd ed.;McGraw-Hill Companies, Inc.: New York, 2006; pp 391, 651.
(37) Aharon, I.; Shaw, B. D. *Microgravity Sci. Technol.* **1997**, *10* (2), 75−85.
(38) Mobil Oil Corp. *Automotive Gasolines*, Report No. 9130-00-142-9457; Mobil Oil Corp.: Fairfax, VA, 1987; available online: http://ww2.ramapo.edu/libfiles/HR/Environmental_Health_and_Safety/MSDS/Facilities/Plumbing/gasoline.pdf